Spaceborne Demonstration of GNSS-R Scattering Cross Section Sensitivity to Wind Direction

Daniel Pascual, *Member, IEEE*, Maria Paola Clarizia, *Senior Member, IEEE*, and Christopher S. Ruf, *Fellow, IEEE*

***Abstract*— This letter investigates the sensitivity of the ocean surface bistatic scattering cross section measured by the Cyclone Global Navigation Satellite System (CYGNSS) to wind direction using the kurtosis of the delay-Doppler map (DDM) samples within a given area. The azimuthal dependence of the kurtosis is modeled by a cosine expansion of the relative wind direction, as is done in scatterometry for the radar cross section. The harmonic coefficients of the model depend on wind speed and incidence angle. Results show a coefficient of determination (R^2) between 0.6 and 0.9 for wind speeds between 4 and 10 m/s and negligible sensitivity outside this range. This study opens the door to the potential of using CYGNSS data for wind direction estimation.**

***Index Terms*— Cyclone Global Navigation Satellite System (CYGNSS), Global Navigation Satellite System Reflectometry (GNSS-R), wind direction.**

I. Introduction

GLOBAL Navigation Satellite System Reflectometry (GNSS-R) comprises a set of techniques that use the reflected GNSS signals over the surface of the Earth for remote sensing applications [1]–[3]. The combination of the receiver and the GNSS satellite can be understood as a bistatic radar (or multistatic if several GNSS satellites are used) with forward scattering. The main observable in GNSS-R is the delay-Doppler map (DDM), defined as the time cross correlation between the reflected signal and a reference one for different Doppler frequencies [1]. Two main techniques exist depending on the reference signal. In conventional GNSS-R (cGNSSR), the reference signal is a locally generated clean replica of a transmitted signal. The interferometric (iGNSS-R) technique uses as reference signal the direct one. In some instruments, the cross correlation between the direct signal and the clean replica is used as well for reference purposes. Another common observable is the so-called waveform, which is a delay cut of the DDM, usually, the one across the DDM peak or across the specular delay [1].

Manuscript received September 29, 2020; revised November 6, 2020; accepted December 21, 2020. This work was jointly supported by the University of Michigan and by Deimos Space UK Limited, under the Contract SUBK00009666 and in part by NASA Science Mission Directorate under Contract NNL13AQ00C with the University of Michigan. *(Corresponding author: Daniel Pascual.)*

Daniel Pascual and Maria Paola Clarizia are with Deimos Space UK Ltd., Harwell OX11 0QR, U.K. (e-mail: daniel.pascual@deimos-space.com; paola.clarizia@deimos-space.com).

Christopher S. Ruf is with the Department of Climate and Space Sciences and Engineering, University of Michigan, Ann Arbor, MI 48109 USA (e-mail: cruf@umich.edu).

Color versions of one or more figures in this letter are available at https://doi.org/10.1109/LGRS.2021.3049526.

Digital Object Identifier 10.1109/LGRS.2021.3049526

In December 2016, NASA's mission Cyclone GNSS (CYGNSS) constellation was launched with eight low Earth orbit (LEO) microsatellites for sea wind mapping. Each CYGNSS satellite has two down-looking antennas, which allows each satellite the measurement of four simultaneous reflections every second in total. This gives CYGNSS constellation a better spatial and temporal resolution than classical sensors (i.e., altimeters, scatterometers, or radiometers). The CYGNSS on-board processors compute incoherently averaged power DDMs using the cGNSS-R technique with GPS L1 C/A signals. The coherent integration time is 1 ms and the original number of incoherent averages (and used for this study) was 1000. The current CYGNSS receivers use 500 averages. Although the main goal behind the CYGNSS mission is to measure wind speed in hurricanes, it has been also used over land for soil moisture and flooding applications [4]. This letter investigates the sensitivity of CYGNSS data to wind direction over the sea surface.

Wind direction over the sea surface has been estimated using spaceborne scatterometers from the late 1970s (e.g., [5]) and polarimetric radiometers from the middle 2000s (e.g., [6]) (although the first evidence using spaceborne radiometers was already stated in the early 1990s [7]). Although polarimetric radiometers obtain the wind direction from the Stokes parameters [6], [7], scatterometers relate the radar cross section with the relative wind direction by using its Fourier cosine series [5]

$$\sigma^0 = \sum_{i=0}^{n} A_i \cos(i \cdot \mathrm{WD}) \tag{1}$$

where WD is the relative wind direction, defined as the angle formed by the wind direction vector with respect to the geodetic north and the azimuthal angle of observation. The coefficients A_i depend on the wind speed U_{10}, incidence angle θ_i, frequency, polarization, and other instrumental parameters. Typically, the cosine series is truncated to the first three coefficients [8, Ch. 20.2]

$$\sigma^0 = A0 + A1\cos(\mathrm{WD}) + A2\cos(2\mathrm{WD}) \tag{2}$$

where A_0 is the offset, or the mean value of σ^0 over the full cycle of wind direction range; A_1 is the upwind/downwind modulation coefficient; and A_2 is the upwind/crosswind coefficient. The actual models used in scatterometers, further fit these three coefficients by using more complex formulas with additional coefficients. In general, $A_0 > A_2 > A_1$, which means that the maximum of σ^0 is found at the upwind

direction and that the value at the downwind direction is a little smaller because of the contribution of the A_1 modulation. For the very same reason, the minima are not exactly at the crosswind directions, but slightly shifted.

A result of the model given in (2) is that there is an ambiguity when retrieving the wind direction, as up to four different wind direction values translate into the same σ^0. Scatterometers address this issue by using simultaneous or almost-simultaneous observations of the same point but with different observation angles and polarizations.

There are two main differences between scatterometers and GNSS-R instruments. First, scatterometers measure backscatter, which is resonant with the capillary waves formed over the ocean surface [2, Ch. 11.3]. This phenomenon, known as Bragg resonance, allows the estimation of the local wind speed. In contrast, the GNSS signals measure forward quasi-specular scatter, which does not experience Bragg resonance and is sensitive to a wider range of wave scales. Second, scatterometers use linear polarization (either VV, HH, VH, HV, or a combination of them). In the case of GNSS-R, the reflected signal over the ocean is mostly left-hand circular polarized (LHCP), although some power is reflected with the right-hand circular polarization (RHCP) (e.g., [9], [10]). In any case, the circular polarizations have in principle less sensitivity to wind direction [8, Ch. 11.5].

This work relates the kurtosis of the DDM samples with the wind direction using the same approach done with scatterometer meaurements of the radar cross section. The kurtosis of the DDM samples tells you how the power is spread around its mean in the power domain. Thus, the kurtosis is, in principle, more robust to instrument parameters (either of the transmitter or the receiver) than the peak power, average power, or similar metrics.

This letter is organized as follows: Section II summarizes previous research done in the GNSS-R field involving wind direction estimates; Section III presents the results from this study conducted on CYGNSS data; and finally, conclusions are given in Section IV.

II. Research Done in GNSS-R

Few studies have approached the sensitivity of GNSS-R signals to wind direction. The first set of works modeled the impact of the wind direction on the waveform shape. In [11], simulated airborne waveforms with $\theta_i = 45°$, $U_{10} = 8$ m/s and h = 10 km, have shown a difference of up to 3 dB between upwind and crosswind directions at a distance of 12 chips from the peak of the waveform derivative. A similar difference was obtained in [12], also with simulated airborne waveforms, but with $\theta_i = 37°$, $U_{10} = 9$ m/s, and h = 1.5 km. The work done in [13], estimated the mean square slope (MSS) by fitting waveforms obtained from an airborne experiment to a geometric optics model. In [14], simulated airborne waveforms with h = 10 km presented similar results. Additionally, it also analyzed the reflected RHCP component and showed that the RHCP and LHCP waveforms present different trailing edges. The difference between both decreases when increasing the incidence angle. However, the RHCP power was about 10 dB below that of the LHCP at the delay gates where the sensitivity to wind direction is larger.

Other works have also investigated the relationship between wind direction and the peak of the DDM or the DDM average (DDMA) and by using the model given in (2). In [15], real airborne waveforms obtained from several satellites were combined in order to estimate the wind direction. The observable was the total reflected power obtained by integrating each waveform. In [16] and [17], the theoretical sensitivity from a spaceborne instrument was studied by using the small slope approximation (SSA) scattering model, and the Elfouhaily and Plant spectral models. Results have shown that sensitivity exists when the scattering direction is away from the specular direction. A dynamic range in azimuthal variability of the scattering cross section of about 2 dB was obtained with $\theta_i = 45°$ (the wind speed was not stated). The latter works also analyzed the reflected RHCP component and found that the power is about 25 dB below that of the LHCP for low incidence angles. In [18], the CYGNSS end-to-end simulator (E2ES) was used for the same purposes. The simulator is based on the KA-GO scattering model and used the Katzberg model [19] to compute the MSS. The results have shown that the dependence was almost unimodal (i.e., $A_2 \ll A_1$), and that the dynamic range was below 0.1 dB for $U_{10} = 5$–7 m/s and $\theta_i = 36.5°$. Different results were obtained in [20], were the dynamic range of simulated DDMAs in a spaceborne scenario, and were between 6 dB ($U_{10} = 2$ m/s and $\theta_i = 25°$) and 2 dB ($U_{10} = 10$ m/s and $\theta_i = 25°$). Finally, in [21], real TDS-1 spaceborne data were analyzed and it was observed that the dependence of the DDM peak to wind direction was unimodal, as the opposite to the bimodal behavior described in (2). Nevertheless, the dynamic range was smaller than 1 dB for a $U_{10} = 9$–10 ms/s and $\theta_i = 20°$–$25°$.

A different approach was done in [22] by analyzing the impact of the wind direction on the symmetry of the DDM. A new pair of observables was used. The first, defined as the angle formed by the peak and the center of mass within a given region. The second, defined as the angle between the center of mass and the DDM skirt and defined as the region whose power is within a certain ratio to the DDM peak. A cosine dependence model different from the one in (2), showed a dynamic range of about 30°. The model was then used in a real airborne campaign. These two observables have also been applied in [23] but by using simulated TDS-1 scenarios. However, the dynamic range of those angles decreased to below 2°. The simulator was also based on the KA-GO and Katzberg models [24]

All the works referred to in this section used GPS L1 C/A signals and the cGNSS-R technique. Finally, it is worth stating here that the retrieval problem has been theoretically investigated in [20] and [25] by combining observations from different satellites and by using multibeam antennas.

III. Analysis Using CYGNSS Data

The common conclusion of the works described in Section II is that the sensitivity of GNSS-R signals to wind direction is not found at the peak of the DDM but away from it, which then includes nonspecular reflection geometries.

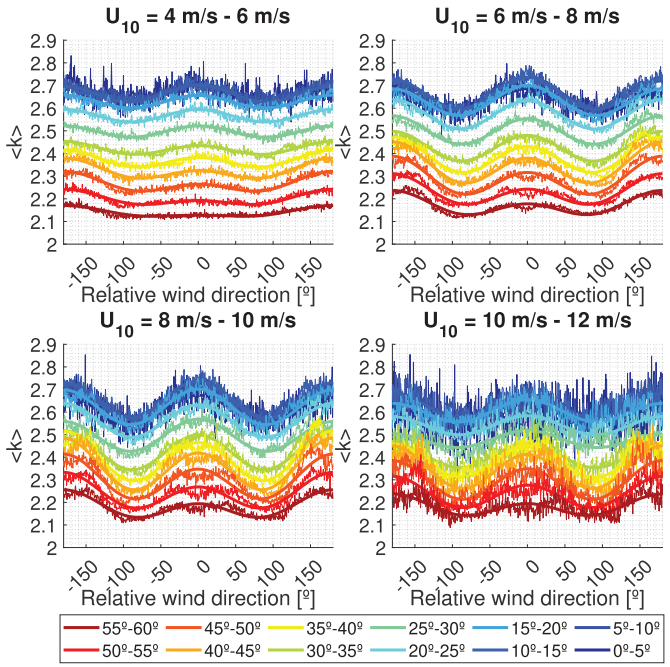

Fig. 1. Sensitivity of kurtosis to wind direction for different wind speeds and incidence angles. Wind direction of ±180° and 0° refers to upwind and downwind, respectively.

In this letter, the analyzed observable is the kurtosis of the DDM samples within a given area near the specular point. The kurtosis is usually interpreted as a measure of the peakedness or tailedness of a distribution. However, a more general concept is that the kurtosis measures the location of the center of mass [26]. More specifically, the kurtosis measures if the mass power is concentrated around the mean or at around the tails. The kurtosis is defined as the fourth central standardized moment as follows:

$$\kappa = \frac{E\left[(x-\mu_x)^4\right]}{\sigma_x^4} \tag{3}$$

where x is the vectorization of the DDM, obtained by stacking one of the two dimensions on top of one another. The fact that kurtosis is a standardized moment, helps the present research as it reduces the impact of calibration and instrument parameters when combining results obtained with different CYGNSS and GPS satellites.

Following the approach outlined for scatterometry, the relationship between kurtosis and wind direction has been modeled for CYGNSS data as in (2):

$$\hat{\kappa} = A_0 + A_1 \cos(\mathrm{WD}) + A_2 \cos(2\mathrm{WD}). \tag{4}$$

The kurtosis values have been obtained from global L1 calibrated DDMs over a six month period (August–December, 2018) [27]. The DDMs are obtained using the cGNSS-R technique using GPS L1 C/A signals and are incoherently averaged over 1 s. The DDM area used to compute the kurtosis is given by ±1500 Hz (three Doppler bins) and ±0.75 C/A chips (three delay lags) referred to as the DDM peak. The fitting model has been applied to kurtosis values averaged in wind direction bins of 0.5° and in cells of $\theta_i = 5°$ and $U_{10} = 2$ m/s. Finally, modeled ocean surface wind speeds and directions output from the WAVEWATCH III (WW3) model [28] with input wind forcing from the European Center for Medium Range Weather Forecast [29] were used as reference data for the wind speed and direction.

Fig. 1 shows some results for wind speeds between 4 and 12 m/s and for the whole range of CYGNSS incident angles (0°–60°). The bimodal dependence can be clearly seen in all cases, as opposed to the results with unimodal dependence obtained when using the DDM peak or DDMA in [18] and [21]. The azimuthal dependence of the kurtosis exhibits a notch in the downwind direction, which is more noticeable for large wind speeds and for large incident angles. This behavior has not previously been observed in the scatterometry or GNSS-R literature. The fitting coefficients are presented in Fig. 2. Except for the A_0 coefficient, there is not a clear common behavior in the curves of each coefficient that could lead to a unified function to fit all of them. Thus, a lookup table is suggested in order not to further increase the overall fitting error. It can be observed that the offset A_0 decreases with increasing incidence angle. The amplitude (mainly given by A_2) increases first with increasing incidence angle up to ≈45° and then decreases. Similarly, the amplitude increases first with increasing wind speed up to ≈10 m/s and then decreases.

The dependence of the kurtosis on wind direction has also been investigated with the kurtosis computed over a larger DDM area away from the specular point. Contrary to what could be expected from the previous theoretical studies, the results show a decrease in sensitivity to the wind direction. This may be caused by the general decrease in bistatic scattering cross section as the measurement geometry deviates more from the specular condition, resulting in that the directional signal, although present, becomes too weak to be observed.

The root mean square error (RMSE) and the coefficient of determination (R^2) metrics, defined as

$$\mathrm{RMSE} = \sqrt{\frac{\sum_{i=1}^{n}(\hat{\kappa}_i - \kappa_i)^2}{n}} \tag{5a}$$

$$R^2 = 1 - \frac{\sum_{i=1}^{n}(\kappa_i - \hat{\kappa}_i)^2}{\sum_{i=1}^{n}(\kappa_i - \bar{\kappa}_i)^2} \tag{5b}$$

are presented in Fig. 3. The model predicts the wind direction dependence with a small error for wind speeds between 4 and 12 m/s. Wind speeds outside this interval show little sensitivity to the wind direction. For low wind speeds, the sea state is calm and the reflection is mostly specular, and thus, less sensitive to the wind direction. For large wind speeds, there are less measurements and they are noisier due to the nature of forward scattering, hence, the direction signal is less evident. Less sensitivity is also observed for small incident angles. An explanation for this can be drawn from [8, Ch. 11.5], where it is shown that the vertical and horizontal polarizations have the same behavior for low incident angles, and thus reducing the sensitivity of the circular polarization. In addition, nadir or quasi-nadir measurements are always less sensitive to the wind direction. Although it is true that the error is smaller for wind speeds between 4 and 12 m/s, it is also true that it is the wind speed region with a larger number of observations

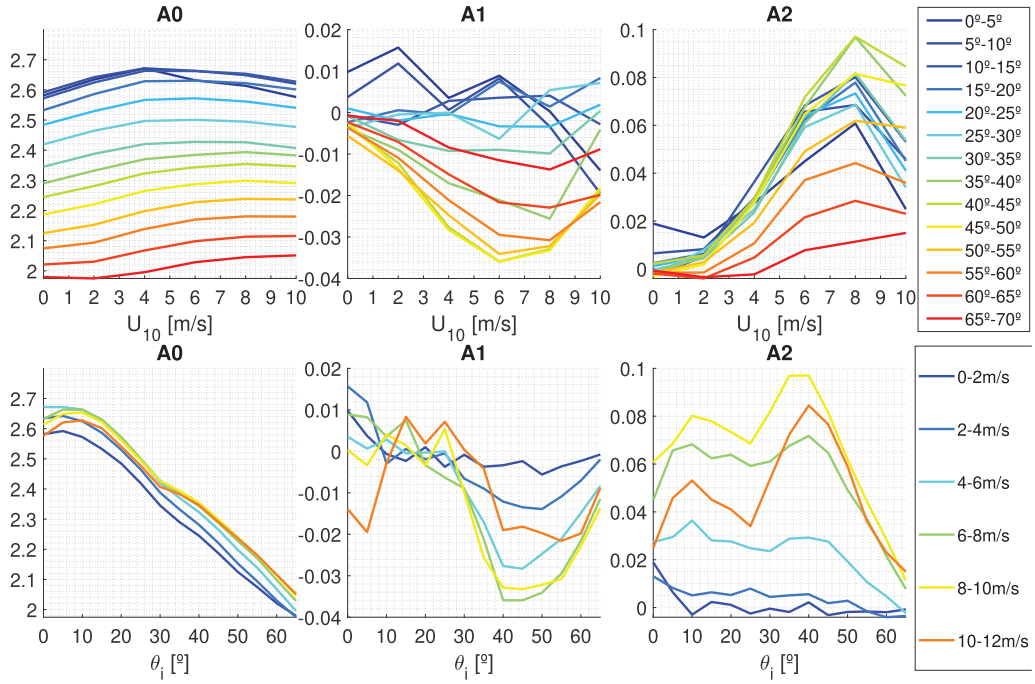

Fig. 2. (Top row) Fitting coefficients shown for different incidence angles and (Bottom row) for different wind speeds.

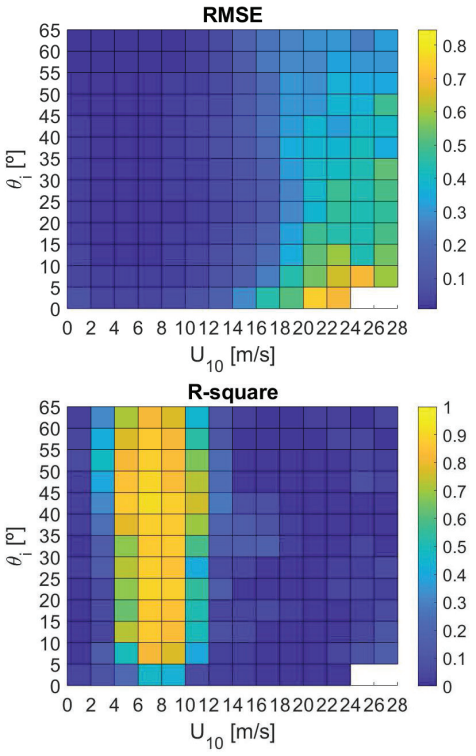

Fig. 3. Fitting error metrics: (Top) rmse and (Bottom) r-square.

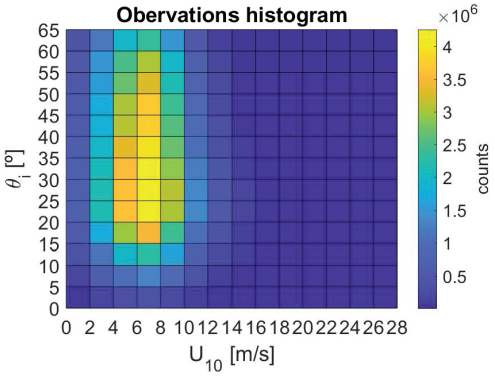

Fig. 4. Number of observations for different wind speeds and incidence angles over a six month period.

(see Fig. 4), and thus where more robust estimates could be obtained.

A general, qualitative comparison can be made with the harmonic coefficients in the CMOD5 model [30], developed for use with the European Remote Sensing (ERS) and Advanced Scatterometer (ASCAT) C-band scatterometers. The A_0 coefficient in CMOD5 also reduces when increasing the incidence angle and exhibits a saturation point with respect to the wind speed, which is near 20 m/s. The A_1 coefficient shows a similar dependence with the incidence angle but with a change of sign. In both models, there is an inflection point at an incidence angle near 40°. Also in both models, the curvature is more pronounced as the wind speed increases. Finally, the A_2 coefficient shows a very similar trend with respect to the wind speed, with its leading edge sharper than the trailing edge, and with a maximum near 10 m/s in both models. Also in both models, the coefficient increases with increasing incidence angle. However, in the model presented here, it decreases again near 45°.

IV. Conclusion

This work has highlighted the sensitivity of CYGNSS data to wind direction, paving the way for potential wind direction estimation from CYGNSS data in the future. The kurtosis of the DDM samples around its peak shows a bimodal dependence on the relative wind direction, and it has been modeled as the cosine series of the relative wind direction. The model depends on the wind speed and on the incidence

angle. Results show that the model agrees well for wind speeds between 4 and 10 m/s and for incident angles larger than 5°, with an R^2 value between 0.6 and 0.9. The best fitting is obtained for wind speeds between 8 and 10 m/s and incidence angles between 30° and 35°.

The cosine dependence translates into ambiguity in the wind direction retrieval. The ambiguity can be reduced and eventually resolved, by combining measurements over the same area and within a short time window, but obtained from different incidence and azimuthal angles. This could be performed by using coincident observations from different CYGNSS satellites.

In principle, the ambiguity could also be reduced by combining measurements obtained with the reflected LHCP and RHCP components if the receiver is capable of receiving both polarizations, which is not the case of the CYGNSS satellites. However, a high directive dual-polarization antenna with large cross-polarization isolation would be needed. In order to give context to the reader, the work done in [10] combined GPS L2C data obtained with the V and H polarizations of the Soil Moisture Active Passive (SMAP) radiometer to form LHCP and RHCP cGNSS-R DDMs (4 ms coherent integration time and five noncoherent averages). Results showed that the DDM peak of the RHCP return was 26 dB below that of the LHCP. Also, the polarization purity of the transmitted GNSS signals should be considered. As a matter of example, the GPS polarization purity degrades (becomes more elliptical) away from the transmitter antenna boresight. In terms of CYGNSS coordinates, the purity is highest for measurements at the lowest incidence angles and degrades at higher incidence angles.

REFERENCES

[1] V. U. Zavorotny, S. Gleason, E. Cardellach, and A. Camps, "Tutorial on remote sensing using GNSS bistatic radar of opportunity," *IEEE Geosci. Remote Sens. Mag.*, vol. 2, no. 4, pp. 8–45, Dec. 2014.

[2] E. Cardellach, F. Xie, and S. Jin, *GNSS Remote Sensing: Theory, Methods and Applications*. Dordrecht, The Netherlands: Springer, 2014.

[3] W. J. Emery and A. Camps, *Introduction to Satellite Remote Sensing: Atmosphere, Ocean, Land and Cryosphere Applications*. Amsterdam, The Netherlands: Elsevier, 2017.

[4] C. Ruf *et al.*, "In-orbit performance of the constellation of CYGNSS hurricane satellites," *Bull. Amer. Meteorol. Soc.*, vol. 100, no. 10, pp. 2009–2023, Oct. 2019.

[5] R. K. Moore and A. K. Fung, "Radar determination of winds at sea," *Proc. IEEE*, vol. 67, no. 11, pp. 1504–1521, Nov. 1979.

[6] P. W. Gaiser *et al.*, "The WindSat spaceborne polarimetric microwave radiometer: Sensor description and early orbit performance," *IEEE Trans. Geosci. Remote Sens.*, vol. 42, no. 11, pp. 2347–2361, Nov. 2004.

[7] F. J. Wentz, "Measurement of oceanic wind vector using satellite microwave radiometers," *IEEE Trans. Geosci. Remote Sens.*, vol. 30, no. 5, pp. 960–972, Sep. 1992.

[8] F. T. Ulaby, R. K. Moore, and A. K. Fung, *Microwave Remote Sensing: Active and Passive*, vols. 1–3. Norwood, MA, USA: Artech House, 1981.

[9] D. Schiavulli, A. Ghavidel, A. Camps, and M. Migliaccio, "GNSS-R wind-dependent polarimetric signature over the ocean," *IEEE Geosci. Remote Sens. Lett.*, vol. 12, no. 12, pp. 2374–2378, Dec. 2015.

[10] M. Buchanan and A. O'Brien, "Investigation of spaceborne polarimetric GNSS-R using the SMAP radar instrument," in *Proc. IEEE Int. Geosci. Remote Sens. Symp. (IGARSS)*, Jul. 2017, pp. 4099–4101.

[11] V. U. Zavorotny and A. G. Voronovich, "Scattering of GPS signals from the ocean with wind remote sensing application," *IEEE Trans. Geosci. Remote Sens.*, vol. 38, no. 2, pp. 951–964, Mar. 2000.

[12] C. Zuffada, T. Elfouhaily, and S. Lowe, "Sensitivity analysis of wind vector measurements from ocean reflected GPS signals," *Remote Sens. Environ.*, vol. 88, no. 3, pp. 341–350, Dec. 2003.

[13] J. L. Garrison, "Anisotropy in reflected GPS measurements of ocean winds," in *Proc. IEEE Int. Geosci. Remote Sens. Symp. (IGARSS)*, Jul. 2003, pp. 4480–4482.

[14] C. Zuffada, A. Fung, J. Parker, M. Okolicanyi, and E. Huang, "Polarization properties of the GPS signal scattered off a wind-driven ocean," *IEEE Trans. Antennas Propag.*, vol. 52, no. 1, pp. 172–188, Jan. 2004.

[15] A. Komjathy, M. Armatys, D. Masters, P. Axelrad, V. Zavorotny, and S. Katzberg, "Retrieval of ocean surface wind speed and wind direction using reflected GPS signals," *J. Atmos. Ocean. Technol.*, vol. 21, no. 3, pp. 515–526, Mar. 2004.

[16] V. U. Zavorotny and A. G. Voronovich, "Recent progress on forward scattering modeling for GNSS reflectometry," in *Proc. IEEE Geosci. Remote Sens. Symp.*, Jul. 2014, pp. 3814–3817.

[17] A. G. Voronovich and V. U. Zavorotny, "Full-polarization modeling of monostatic and bistatic radar scattering from a rough sea surface," *IEEE Trans. Antennas Propag.*, vol. 62, no. 3, pp. 1362–1371, Mar. 2014.

[18] J. Park and J. T. Johnson, "A study of wind direction effects on sea surface specular scattering for GNSS-R applications," *IEEE J. Sel. Topics Appl. Earth Observ. Remote Sens.*, vol. 10, no. 11, pp. 4677–4685, Nov. 2017.

[19] S. J. Katzberg, J. Dunion, and G. G. Ganoe, "The use of reflected GPS signals to retrieve ocean surface wind speeds in tropical cyclones," *Radio Sci.*, vol. 48, no. 4, pp. 371–387, Jul. 2013.

[20] G. Zhang, D. Yang, Y. Yu, and F. Wang, "Wind direction retrieval using spaceborne GNSS-R in nonspecular geometry," *IEEE J. Sel. Topics Appl. Earth Observ. Remote Sens.*, vol. 13, pp. 649–658, 2020.

[21] S. Soisuvarn, Z. Jelenak, F. Said, P. S. Chang, and A. Egido, "The GNSS reflectometry response to the ocean surface winds and waves," *IEEE J. Sel. Topics Appl. Earth Observ. Remote Sens.*, vol. 9, no. 10, pp. 4678–4699, Oct. 2016.

[22] E. Valencia, V. U. Zavorotny, D. M. Akos, and A. Camps, "Using DDM asymmetry metrics for wind direction retrieval from GPS ocean-scattered signals in airborne experiments," *IEEE Trans. Geosci. Remote Sens.*, vol. 52, no. 7, pp. 3924–3936, Jul. 2014.

[23] D. Guan *et al.*, "Wind direction signatures in GNSS-R observables from space," *Remote Sens.*, vol. 10, no. 2, p. 198, Jan. 2018.

[24] H. Park *et al.*, "A generic level 1 simulator for spaceborne GNSS-R missions and application to GEROS-ISS ocean reflectometry," *IEEE J. Sel. Topics Appl. Earth Observ. Remote Sens.*, vol. 10, no. 10, pp. 4645–4659, Oct. 2017.

[25] F. Wang, D. Yang, and L. Yang, "Feasibility of wind direction observation using low-altitude global navigation satellite system-reflectometry," *IEEE J. Sel. Topics Appl. Earth Observ. Remote Sens.*, vol. 11, no. 12, pp. 5063–5075, Dec. 2018.

[26] L. T. DeCarlo, "On the meaning and use of kurtosis," *Psychol. Methods*, vol. 2, no. 3, pp. 292–307, 1997.

[27] (2020). *CYGNSS Level 1 Full Delay Doppler Map Data Record*. [Online]. Available: https://podaac.jpl.nasa.gov/dataset/CYGNSS_L1_FULL_DDM

[28] H. L. Tolman, "User manual and system documentation of WAVEWATCH III version 3.14," NOAA, Camp Springs, MD, USA, Tech. Rep. 3.14, 2009. [Online]. Available: http://nopp.ncep.noaa.gov/mmab/papers/tn276/MMAB_276.pdf

[29] E. Andersson, A. Persson, and I. Tsonevsky, "User guide to ECMWF forecast products," ECMWF, Reading, U.K., Tech. Rep. 2.1, 2015, vol. 2.1.

[30] H. Hersbach, A. Stoffelen, and S. de Haan, "An improved C-band scatterometer ocean geophysical model function: CMOD5," *J. Geophys. Res.*, vol. 112, no. C3, pp. 1–18, Mar. 2007.